FERMILAB-CONF-76-129-E E118A

Paper Submitted to the

XVIII International Conference on High Energy Physics

# Energy and Target Dependence of the Pseudo-Rapidity Distributions in Pion- and Proton- Nucleus Collisions at Fermilab Energies*

by

W. Busza, D. Luckey, L. Votta, C. Young,
Massachusetts Institute of Technology, Massachusetts U.S.A.
C. Halliwell, Carleton University, Ontario, Canada
J. Elias, Fermi National Accelerator Laboratory, Illinois, USA

Multiparticle production in hadron-nucleus collisions has been studied using hodoscope arrays. Data on angular distributions were collected for incident $\pi^{\pm}$, $K^{\pm}$, and $P^{\pm}$ at 50,100, and 200 GeV with targets ranging from hydrogen through uranium. We observe that the extent in pseudo-rapidity of particles produced in the target fragmentation region increases with energy. Proton and pion induced reactions exhibit different behavior for the same target nucleus. However, for target nuclei with identical values of $\bar{\nu}$, (where $\bar{\nu}$ is the average thickness in units of the mean free path of the incident particle) the behavior is similar. Pseudo-rapidity distributions are compared with theoretical models.

* Work supported in part by the United States E.R.D.A. under Contract No. E(11-1)-3069, the National Science Foundation, and the National Research Council of Canada.

It is well established that hadronic interactions take significant time to develop.[1,2] The use of nuclear targets is ideally suited to probe this development.[1] There exists a class of theoretical models which agree with the overall features of hadron-nucleus interactions.[2,3] These features include:

i) the energy independence of $R_A$ measured in proton-emulsion interactions[4]. $R_A$ is the ratio of mean charged multiplicities in hadron-nucleus and hadron-proton collisions.

ii) the apparent similarity of pion- and proton- induced reactions[1] (when $\bar{\nu}$, the average nuclear thickness measured in units of the absorption mean free path of the incident hadron is considered the relevant parameter);

iii) the observation that the charged multiplicity of secondaries with a large value of pseudo-rapidity[5], $\eta$, is independent of target.[1] For small values of $\eta$ the multiplicity is approximately proportional to $\bar{\nu}$.[6]

However, no detailed information on the energy and target dependence of hadron-nucleus interactions has been available prior to this experiment. Such information is needed in order to differentiate between the various proposed mechanisms of multiparticle production. To obtain quantitative information concerning ii) and iii) above, pseudo-rapidity distributions were studied using a tagged charged hadron beam of both polarities. Data were collected at 50, 100, and 200 GeV with targets consisting of $CH_2$, Be, C, Al, Ti, Emulsion, Cu, Mo, Ag, W, Pb, and U.

Targets of several lengths were used for each material to permit an extrapolation to zero target length. In order to measure the multiplicity of secondaries as a function of $\eta$, wide angle products of the interaction were detected in four lucite hodoscopes. Forward products were counted in a high resolution lucite Cerenkov counter using pulse height techniques.[7] The use of lucite imposed a selection of velocities greater than 0.85c. No neutrals were intentionally detected and no identification of charged secondaries was carried out.

The apparatus (see Fig. 1) was triggered when either one particle at a wide angle or two or more forward particles resulted from an interaction.

In the data analysis events were rejected which contained less than 3 particles or in which counter V3 fired. V3 subtended a solid angle of $\sim$ 2$\mu$ster. which corresponds to $\eta \gtrsim 7$. In addition to the extrapolation to zero target thickness, corrections were applied for secondary interactions, $\gamma$-conversions from $\pi^0$'s, $\delta$-rays, acceptance, etc. The missing 0,1, and 2 particle events were estimated by comparing the measured interaction rates with known absorption cross sections.[8]

Typical data are shown in Figs. 2(a) - 2(e). As can be seen the variation of the multiplicity per unit $\eta$ interval with $\bar{\nu}$ is a strong function of $\eta$. This effect is most apparent in Fig. 2(f).

Figure 3(a) shows the variation of $R_A$ with $\bar{\nu}$ for pion and

proton interactions. No significant difference is seen for the energy range 50 $\rightarrow$ 200 GeV. A smooth line through the data is shown in Fig. 3(b) where, for comparison, $R_A = 1/2 + 1/2\bar{\nu}$ is indicated. Table I summarizes these data.

The energy dependence of $R_A$ for various targets and different incident particles is displayed in Fig. 4. In addition, the emulsion data from this experiment are compared with the world average data.[4] No significant energy dependence is evident from 50 to 200 GeV.

Pseudo-rapidity distributions for protons and pions are compared in Figs. 5(a) - 5(c). Although $R_A$ seems to be particle independent, Fig. 5 indicates that there are small differences in the $\eta$ distributions.

Figure 6 shows the variation with energy of the $\eta$ distributions for carbon and lead. For $\eta \lesssim 1.5$ little dependence on energy is seen. There is an increase in the width of the distribution for both carbon and lead.

$\eta$ distributions as a function of $\bar{\nu}$ are shown in Fig. 7 for protons at 200 GeV. For $\bar{\nu} > 1$ little or no increase is seen over hydrogen data for the region $\eta \gtrsim 4.0$. The peak of the distribution moves to a lower value of pseudo-rapidity for increasing values of $\bar{\nu}$.[9]

Specific predictions concerning the energy and $\bar{\nu}$ dependence of the rapidity distribution vary from theory to theory. The multiperipheral model predicts that, at constant energy, the height of the rapidity distribution in hadron-nucleus interactions

should increase (compared with hydrogen) over the full rapidity range, especially in the backward region.[10] The data show no appreciable difference for $\eta \gtrsim 4$. (Fig. 8). Although there is an enhancement in the lower rapidity region, the extent of this increase is not energy independent as the model requires.[2] This is shown in Fig. 9 where an increase of $\sim$1 rapidity unit occurs in pion-lead data between 50 and 200 GeV. On the other hand, the energy flux cascade model[11] predicts a variation of this type. For a given energy the latter theory restricts the enhancement at lower rapidities to a region independent of $\bar{\nu}$. This effect is seen in Fig. 8. The predictions of the coherent tube model[12] are compared with data in Fig. 10. Although the peak of the rapidity distribution moves to lower values of $\eta$ in accordance with this model, the data are not in good agreement.

In conclusion, we find that the data most strongly support a description of multiparticle production of the hydrodynamical (or energy-flux) type. However, the data have features of a variety of mechanisms; for example, there is evidence of the occurrence of at least some cascading of the particles produced in the target fragmentation region; there are also indications that the effective center of mass system in hadron-nucleus collisions is not identical to that in hadron-hadron collisions. It is now important to study carefully the restrictions which these data place on the possible mechanisms of particle production.

We thank the Fermilab staff for their cooperation and assistance. The help of the staff of the Laboratory for Nuclear

Science at the Massachusetts Institute of Technology is greatly appreciated, in particular that of Craig Bolon, Tommy Lyons, and Cy Tourtellotte. One of us (Clive Halliwell) wishes to express his appreciation to E.P. Hincks for support and encouragement. Finally, the collaboration from MIT wishes to thank their colleagues at MIT for valuable discussions and constant support.

TABLE I

Mean Multiplicities, $\langle n \rangle$, of Charged Secondaries ($\beta \gtrsim 0.85$) in in Hadron-Nucleus Collisions

| | | $\pi^+$ | | $\pi^+$ | | $\pi^-$ | |
|---|---|---|---|---|---|---|---|
| | | 50 GeV | | 100 GeV | | 200 GeV | |
| $\bar{\nu}_\pi$ | Element | $\langle n \rangle$ | $R_A$ | $\langle n \rangle$ | $R_A$ | $\langle n \rangle$ | $R_A$ |
| 1.00 | $H_2$ | 5.5 | 1.00 | 6.6 | 1.00 | 7.8 | 1.00 |
| 1.39 | C | 6.5 | 1.19 | 7.8 | 1.18 | 9.3 | 1.19 |
| 1.70 | Al | 7.4 | 1.34 | 8.8 | 1.33 | 10.5 | 1.35 |
| 2.00 | ---* | 8.3 | 1.51 | 9.9 | 1.49 | 11.8 | 1.52 |
| 2.10 | Cu | 8.6 | 1.56 | 10.2 | 1.55 | 12.3 | 1.58 |
| 2.40 | Ag | 9.6 | 1.74 | 11.5 | 1.73 | 13.8 | 1.77 |
| 2.82 | Pb | 11.1 | 2.00 | 13.3 | 2.01 | 16.2 | 2.07 |
| 3.00 | ---* | 11.7 | 2.12 | 14.2 | 2.14 | 17.5 | 2.24 |
| $\bar{\nu}_p$ | | | | $p^+$ | | $p^+$ | |
| | | | | 100 GeV | | 200 GeV | |
| 1.00 | $H_2$ | | | 6.2 | 1.00 | 7.4 | 1.00 |
| 1.52 | C | | | 7.8 | 1.27 | 9.4 | 1.28 |
| 1.95 | Al | | | 9.3 | 1.50 | 11.2 | 1.52 |
| 2.00 | ---* | | | 9.4 | 1.53 | 11.4 | 1.55 |
| 2.54 | Cu | | | 11.2 | 1.82 | 13.5 | 1.84 |
| 3.00 | Ag | | | 12.7 | 2.06 | 15.5 | 2.11 |
| 3.67 | Pb | | | 14.9 | 2.41 | 18.6 | 2.53 |
| 4.00 | ---* | | | 16.1 | 2.61 | 20.3 | 2.76 |

All errors $\gtrsim \pm$ 3%.

* Values interpolated from the observed $\bar{\nu}$ dependences as shown for example, in Fig. 2.

## REFERENCES


1. W. Busza, Proceedings of the VIth International Conference on High Energy Physics and Nuclear Structure, Santa Fe and Los Alamos, 1975.

2. L. Bertocchi, Proceedings of the VIth International Conference on High Energy Physics and Nuclear Structure, Santa Fe and Los Alamos, 1975.

3. K. Gottfried, Vth International Conference on High Energy Physics and Nuclear Structure, Lund, 1973.

4. J. Babecki, Acta Physica Polonica, B6, No.3, 443 (1975).

5. Pseudo-rapidity $\eta \equiv -\ell n(\tan {}^{\theta}L/2)$ is a good approximation to the rapidity:

$$y = \ell n\left(\frac{E+P_{\parallel}}{E-P_{\parallel}}\right) \text{ when } P_{\perp}^{2} >> m^{2}.$$

6. W. Busza et al., Phys. Rev. Lett. 34, 838 (1975).

7. W. Busza, Proceedings of the Topical Meeting on High Energy Collisions Involving Nuclei, Trieste, Italy, September, 1974.

8. S. Denisov et al., Nucl. Phys. B61, 62 (1973).

9. This effect is also apparent in the chromium and tungsten data of J.R. Florian et al., Phys. Rev. D13, 558 (1976).

10. J. Koplick and A.H. Mueller, Phys. Rev. D12, 3638 (1975).

11. K. Gottfried, Phys. Rev. Lett. 32, 957 (1974).

12. Y. Afek et al.,

## FIGURE CAPTIONS

1. Experimental layout. Each of the 3 ring hodoscopes consisted of 2 layers of 6 counters, the 2 layers being rotated by $30^{\circ}$ with respect to one another which resulted in 12 azimuthal segments.

2. Summary of 200 GeV $P^+$ data. (a) - (e) show the variation of $\Delta N/\Delta\eta$ vs. $\bar{\nu}$ for different ranges of $\eta$. The lines are best estimates of these dependences. (f) is a summary of these data. The left-hand scale is for the solid lines; the right hand scale is for the dashed line. See text for definitions of $\eta$ and $\bar{\nu}$.

3. (a) Variation of $R_A$ with $\bar{\nu}$.

   (b) Smooth line through the data with indication of error at $\bar{\nu}=3.5$. The line $R_A = 1/2 + 1/2\nu$ is also shown.

4. Energy dependence of $R_A$ for various targets.

   (a) Incident protons at 50, 100, and 200 GeV.

   (b) Incident $\pi^+$ at 50 and 100 GeV and $\pi^-$ at 200 GeV.

   (c) Proton-emulsion over the energy range 25 to 300 GeV. The world emulsion data are taken from Reference 4.

5. Comparison of 200 GeV $P^+$ and $\pi^-$ pseudo-rapidity distributions at the same values of $\bar{\nu}$. All errors on pseudo-rapidity distributions are $\tilde{\sim}$ ±4%.

   (a) $\bar{\nu} = 1$; (b) $\bar{\nu} = 2$; (c) $\bar{\nu} = 3$.

6. Energy dependence of pseudo-rapidity distributions for incident pions.
   (a) Carbon target.
   (b) Lead target.

7. Variation of the pseudo-rapidity distribution with $\bar{\nu}$ for proton-induced reactions at 200 GeV. Four values of $\bar{\nu}$ are shown: 1 (i.e., hydrogen), 2,3, and 4.

8. Variation of the pseudo-rapidity distribution with $\bar{\nu}$ for proton-induced reactions at 200 GeV after subtracting hydrogen ($\bar{\nu} = 1$) data.

9. Variation of the pseudo-rapidity distribution with the energy of the incident particle after the subtraction of hydrogen data.

10. Comparison of data with the coherent-tube model. The dotted line shows the theoretical prediction from Ref. 12 for emulsion. The rapidity scale ($y_{Lab.}$) refers to the theoretical prediction; the pseudo-rapidity ($\eta$) to the experimental data.

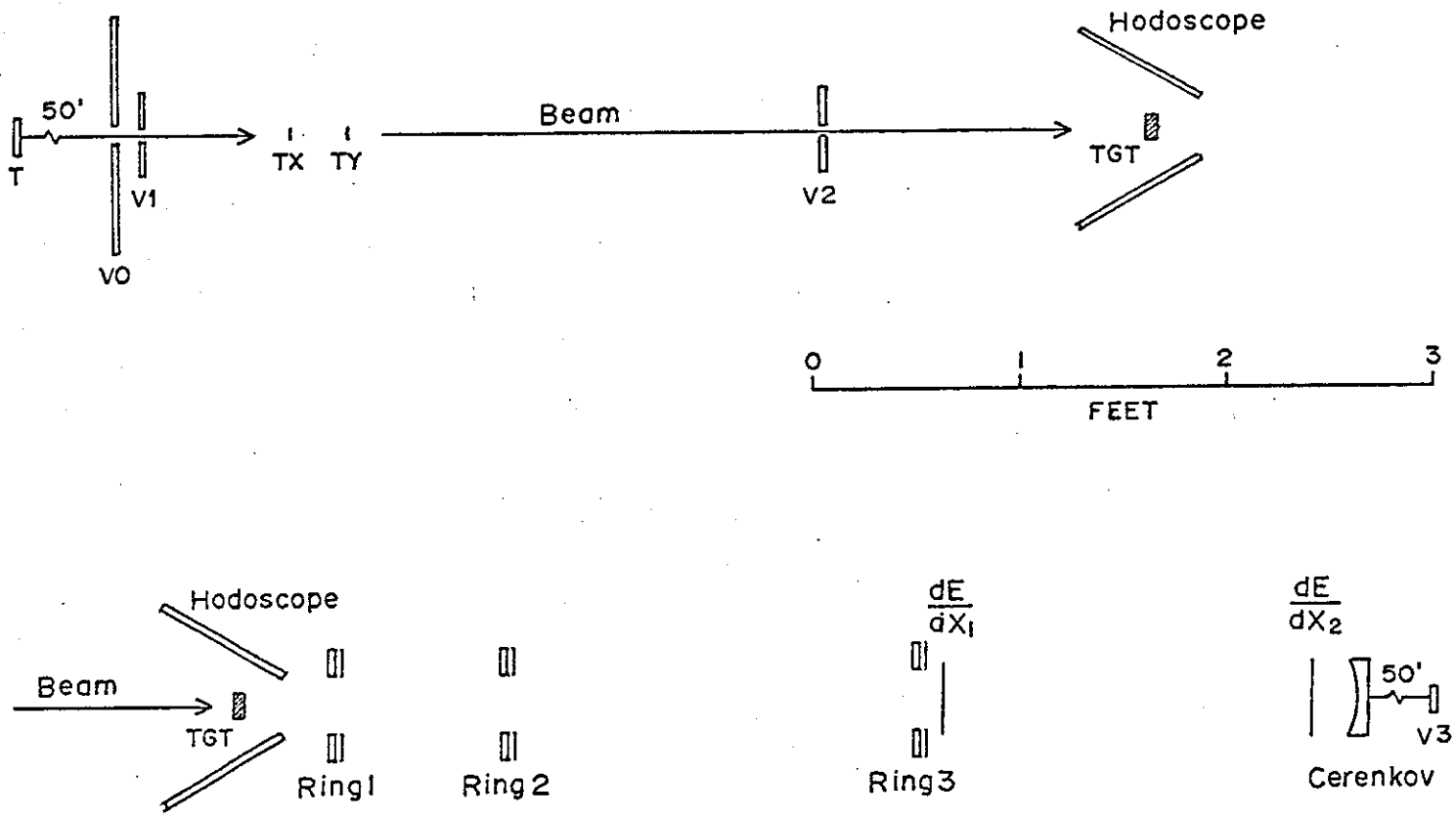
Hodoscope
50'
Beam
T
TX
TY
V1
V0
V2
TGT
0
1
2
3
FEET
Hodoscope
Beam
TGT
Ring1
Ring2
dE/dX1
Ring3
dE/dX2
50'
V3
Cerenkov

Fig. 1

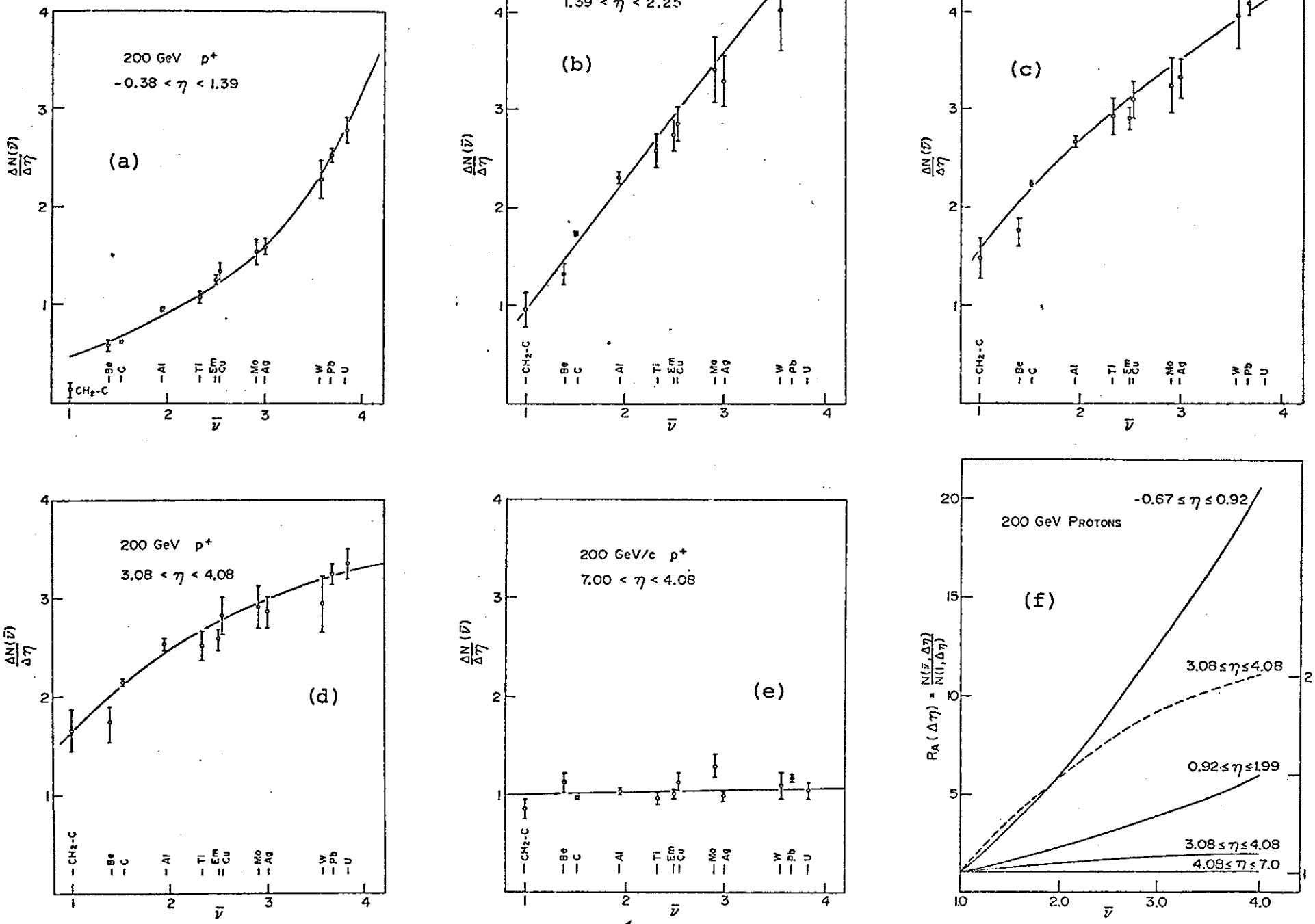
200 GeV p+
-0.38 < η < 1.39
(a)
200 GeV p+
1.39 < η < 2.25
(b)
200 GeV p+
2.25 < η < 3.08
(c)
200 GeV p+
3.08 < η < 4.08
(d)
200 GeV/c p+
7.00 < η < 4.08
(e)
200 GeV Protons
-0.67 ≤ η ≤ 0.92
3.08 ≤ η ≤ 4.08
0.92 ≤ η ≤ 1.99
3.08 ≤ η ≤ 4.08
4.08 ≤ η ≤ 7.0
(f)
CH2-C
Be
C
Al
Ti
Em
Cu
Mo
Ag
W
Pb
U
ν̄

Fig. 2

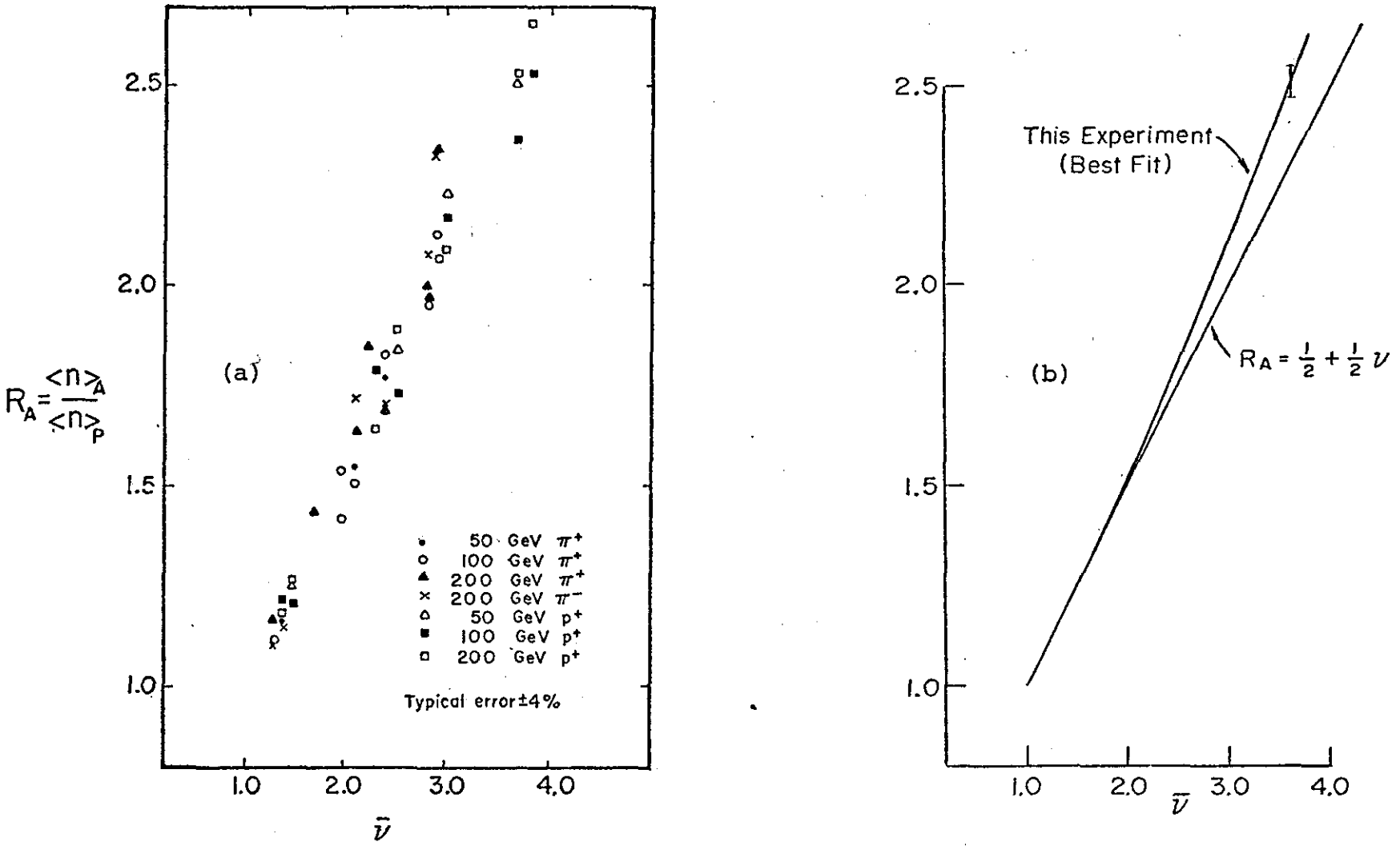
(a)
$R_A = \frac{\langle n \rangle_A}{\langle n \rangle_p}$
2.5
2.0
1.5
1.0
1.0
2.0
3.0
4.0
$\bar{\nu}$
50 GeV $\pi^+$
100 GeV $\pi^+$
200 GeV $\pi^+$
200 GeV $\pi^-$
50 GeV $p^+$
100 GeV $p^+$
200 GeV $p^+$
Typical error±4%
(b)
This Experiment
(Best Fit)
$R_A = \frac{1}{2} + \frac{1}{2}\nu$
2.5
2.0
1.5
1.0
1.0
2.0
3.0
4.0
$\bar{\nu}$

Fig. 3

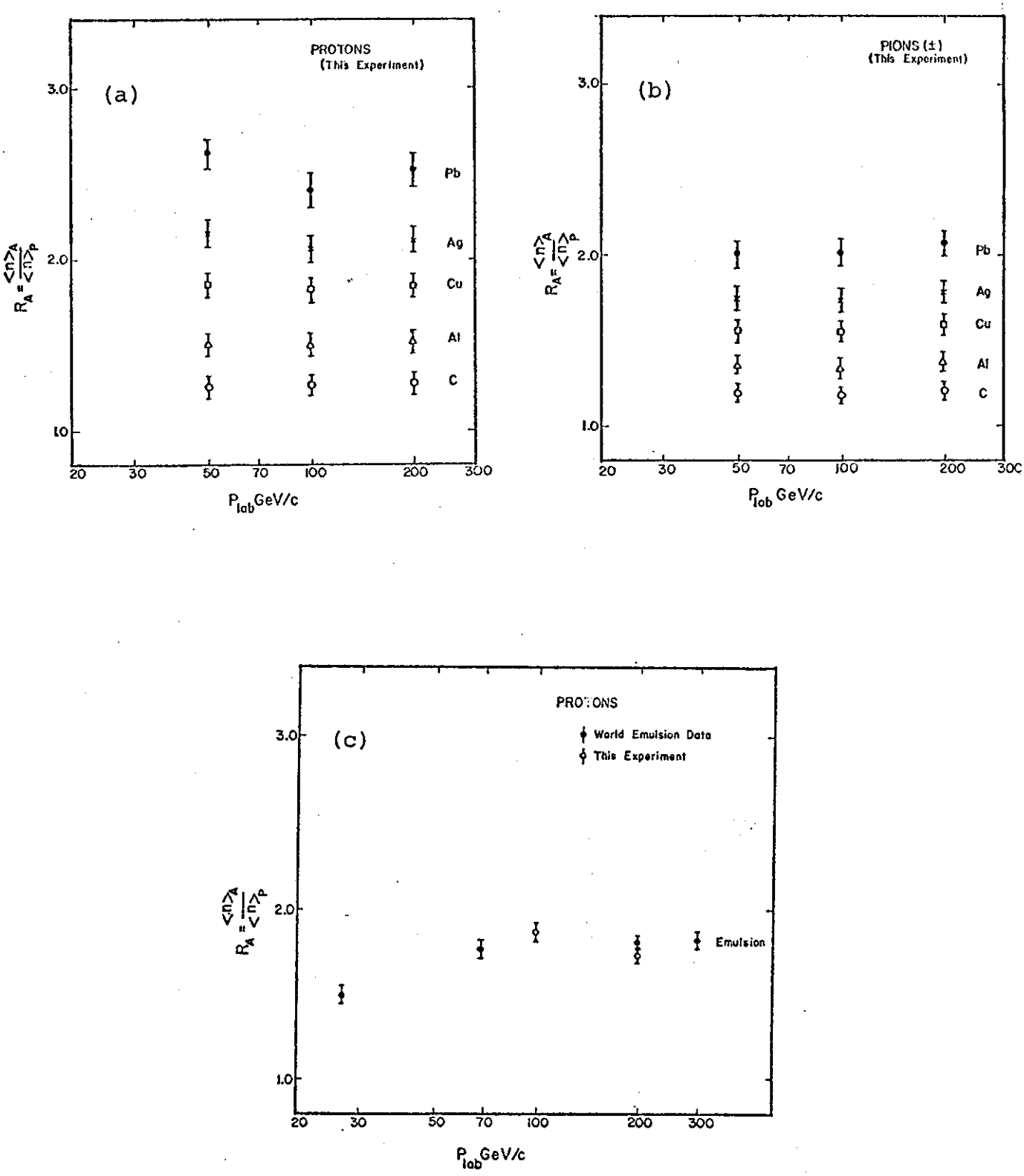
PROTONS
(This Experiment)
(a)
3.0
2.0
1.0
Pb
Ag
Cu
Al
C
20
30
50
70
100
200
300
$P_{lab}$ GeV/c
$R_A = \frac{\langle n \rangle_A}{\langle n \rangle_p}$
PIONS (±)
(This Experiment)
(b)
PROTONS
(c)
World Emulsion Data
This Experiment
Emulsion

Fig. 4

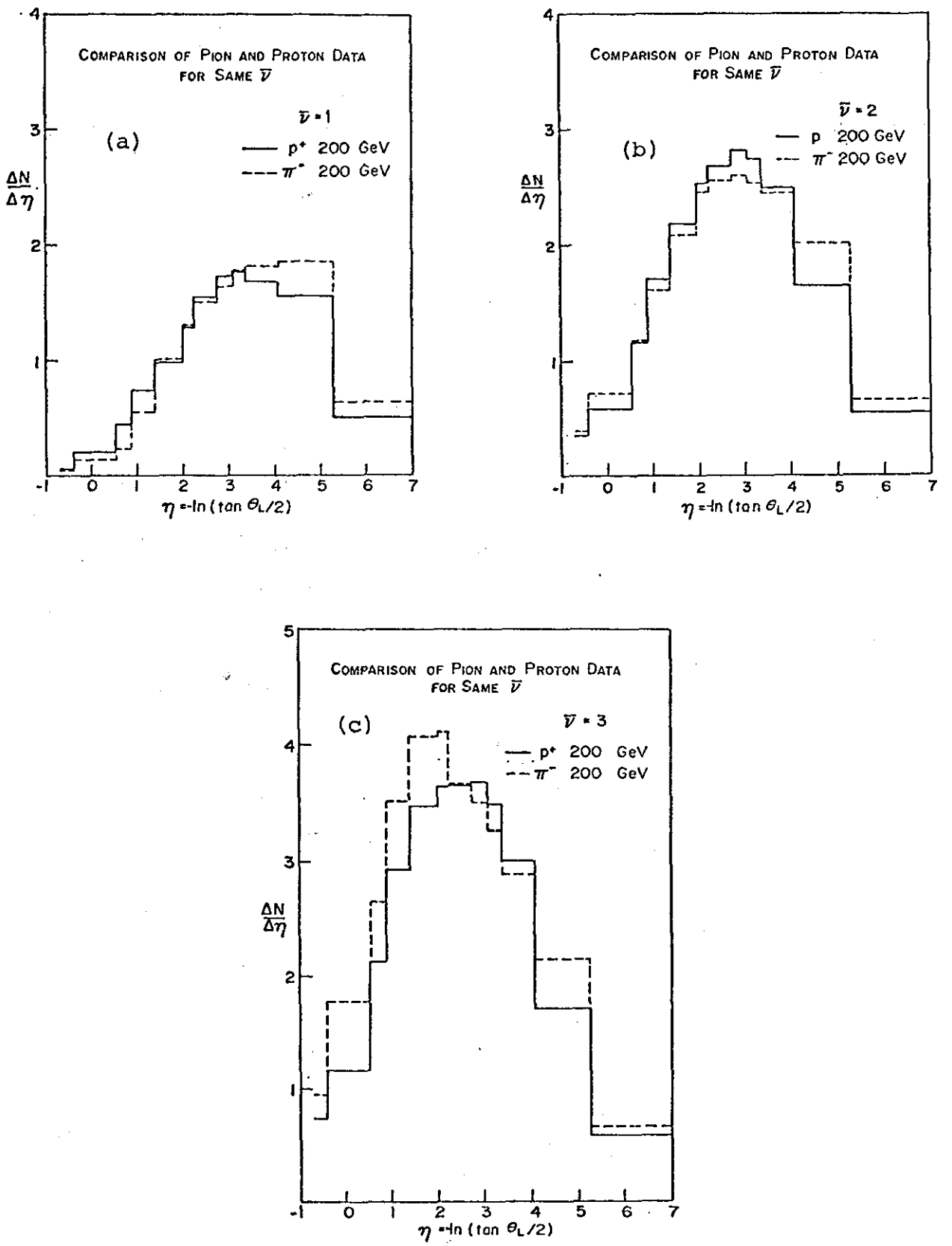
COMPARISON OF PION AND PROTON DATA FOR SAME $\bar{\nu}$
(a)
$\bar{\nu}$ = 1
p⁺ 200 GeV
π⁻ 200 GeV
$\frac{\Delta N}{\Delta \eta}$
$\eta$ = -ln (tan $\theta_L/2$)
COMPARISON OF PION AND PROTON DATA FOR SAME $\bar{\nu}$
(b)
$\bar{\nu}$ = 2
p 200 GeV
π⁻ 200 GeV
$\frac{\Delta N}{\Delta \eta}$
$\eta$ = -ln (tan $\theta_L/2$)
COMPARISON OF PION AND PROTON DATA FOR SAME $\bar{\nu}$
(c)
$\bar{\nu}$ = 3
p⁺ 200 GeV
π⁻ 200 GeV
$\frac{\Delta N}{\Delta \eta}$
$\eta$ = -ln (tan $\theta_L/2$)

Fig. 5

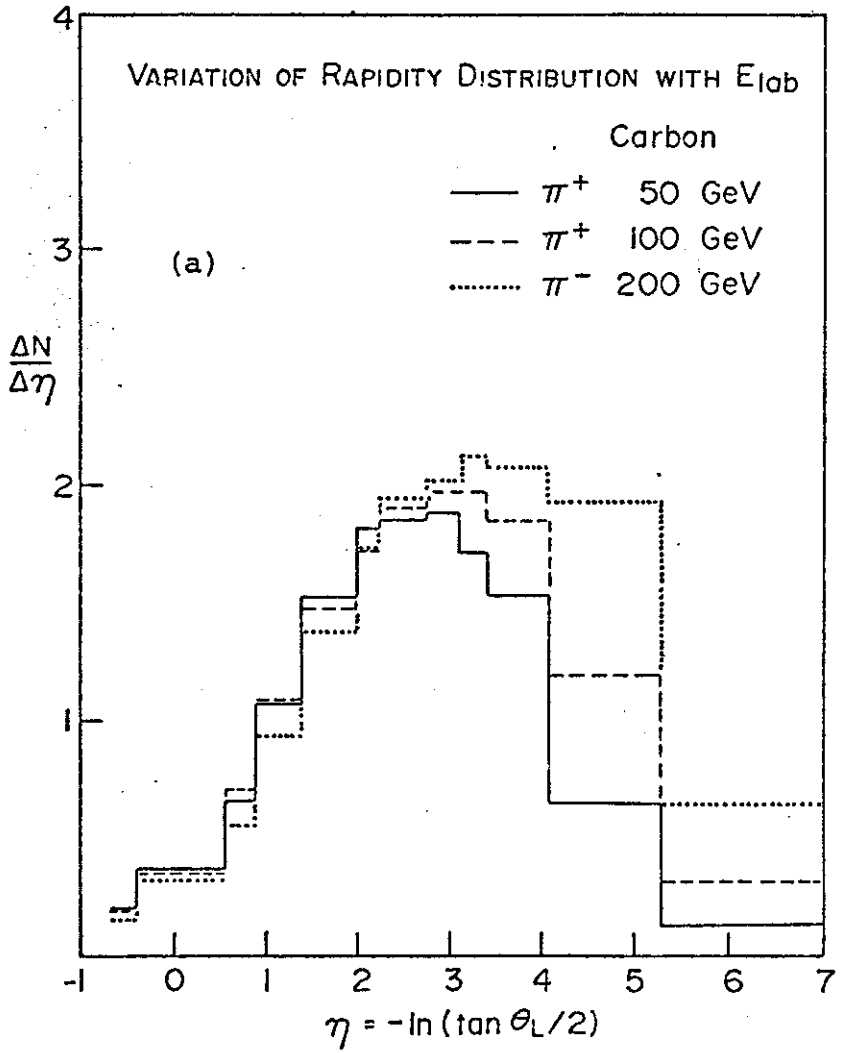
VARIATION OF RAPIDITY DISTRIBUTION WITH $E_{lab}$
Carbon
(a)
$\pi^+$ 50 GeV
$\pi^+$ 100 GeV
$\pi^-$ 200 GeV
$\frac{\Delta N}{\Delta \eta}$
$\eta = -\ln(\tan\theta_L/2)$

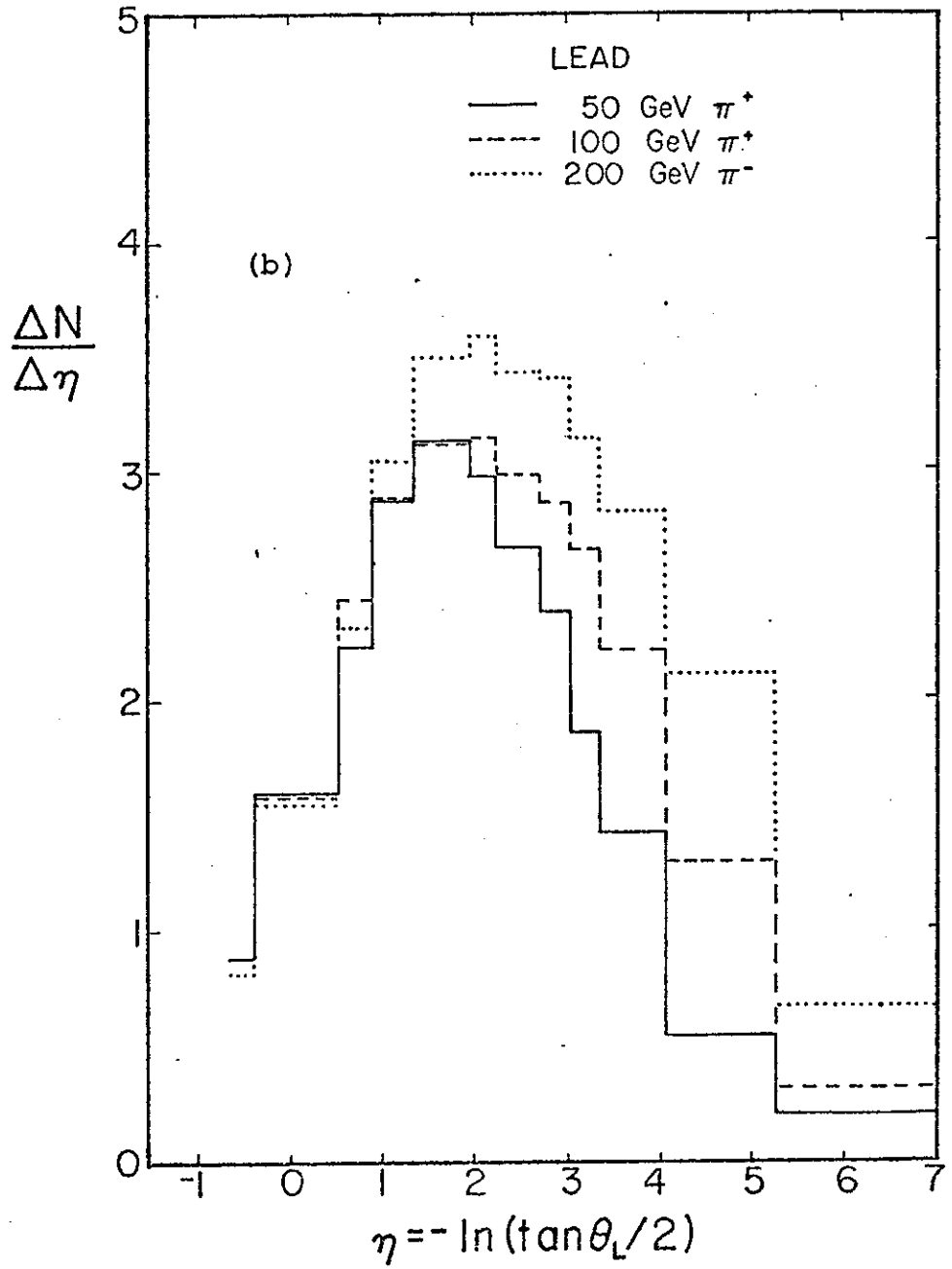
LEAD
50 GeV $\pi^+$
100 GeV $\pi^+$
200 GeV $\pi^-$
(b)
$\frac{\Delta N}{\Delta \eta}$
$\eta = -\ln(\tan\theta_L/2)$

Fig 6

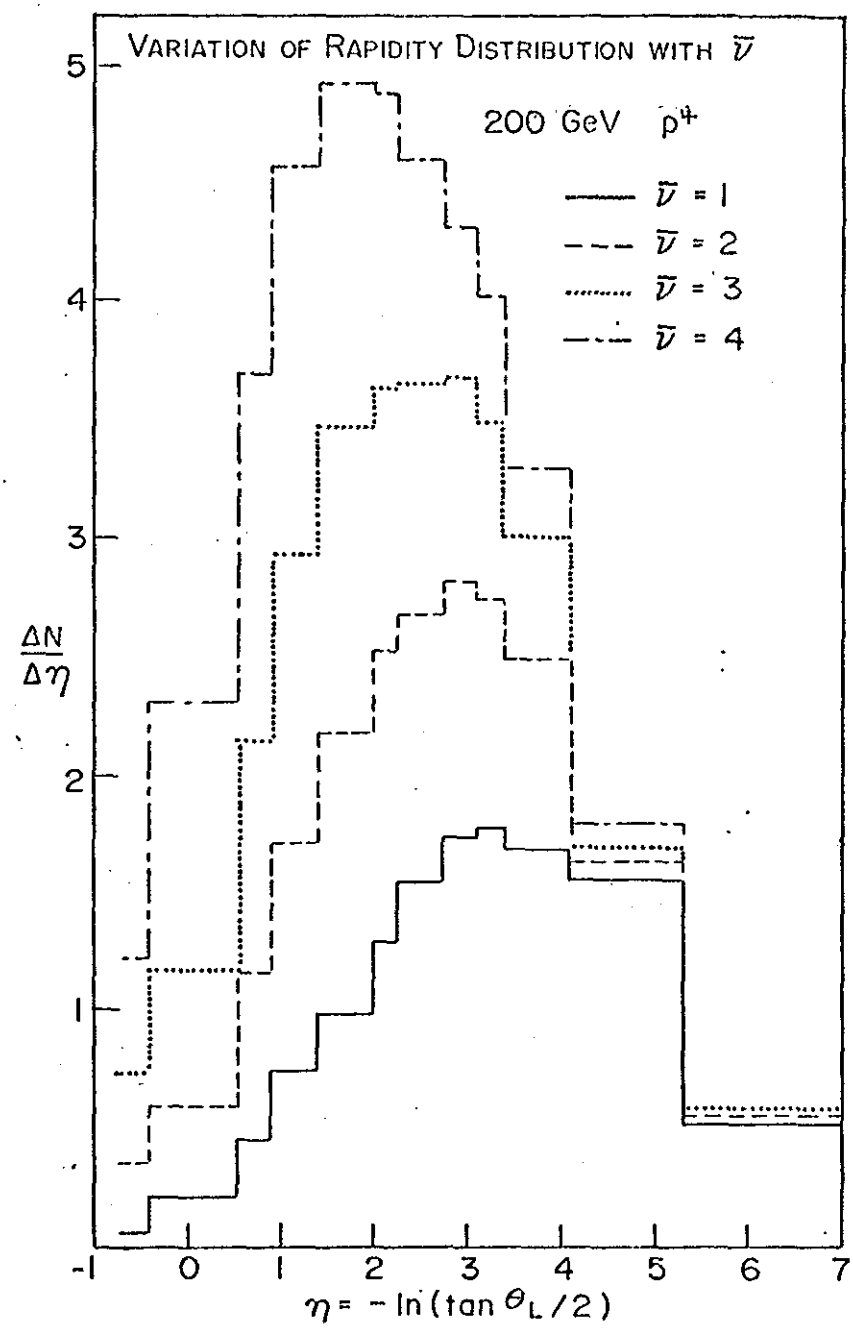
VARIATION OF RAPIDITY DISTRIBUTION WITH $\bar{\nu}$
200 GeV $p^+$
$\bar{\nu}$ = 1
$\bar{\nu}$ = 2
$\bar{\nu}$ = 3
$\bar{\nu}$ = 4
$\frac{\Delta N}{\Delta \eta}$
5
4
3
2
1
-1
0
1
2
3
4
5
6
7
$\eta = -\ln(\tan \theta_L/2)$

Fig. 7

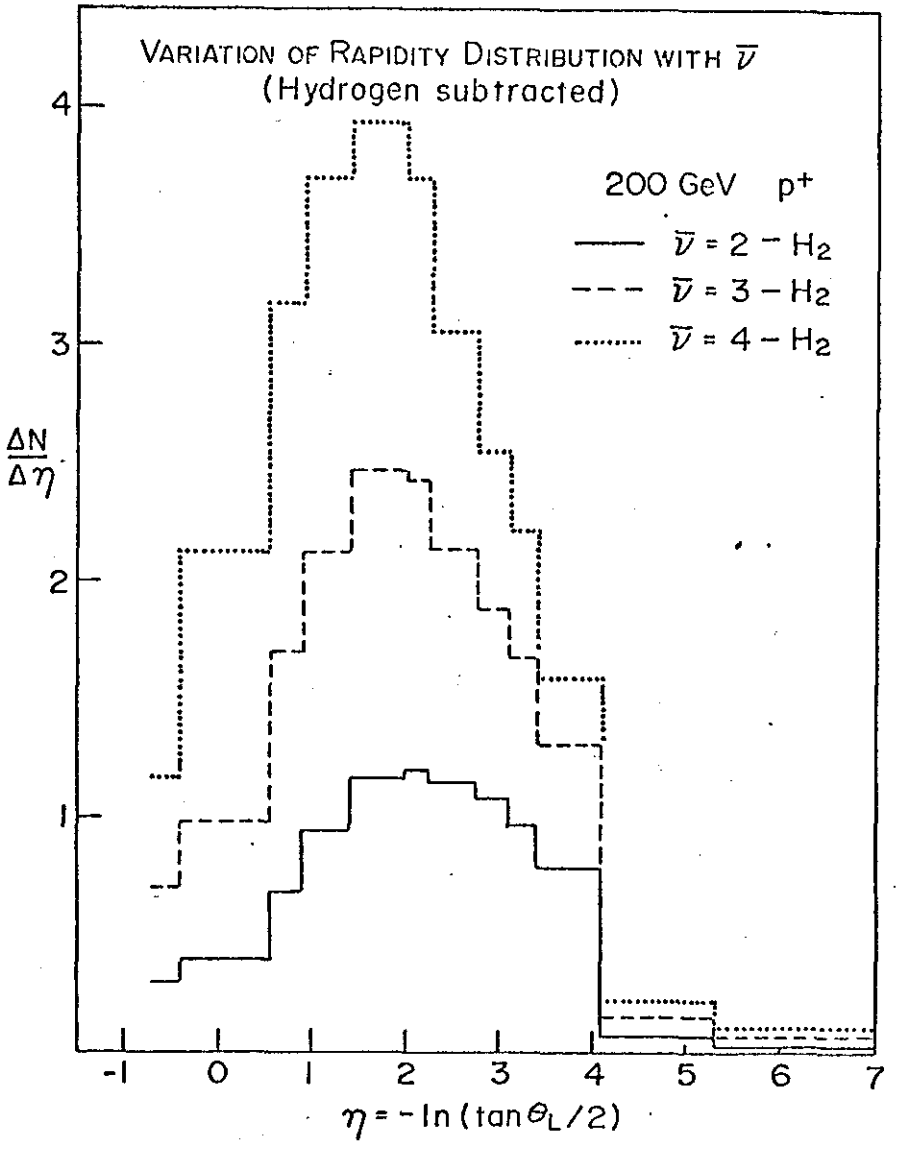
VARIATION OF RAPIDITY DISTRIBUTION WITH $\bar{\nu}$
(Hydrogen subtracted)
200 GeV p+
$\bar{\nu} = 2 - H_2$
$\bar{\nu} = 3 - H_2$
$\bar{\nu} = 4 - H_2$
$\frac{\Delta N}{\Delta \eta}$
$\eta = -\ln(\tan\theta_L/2)$

Fig. 8

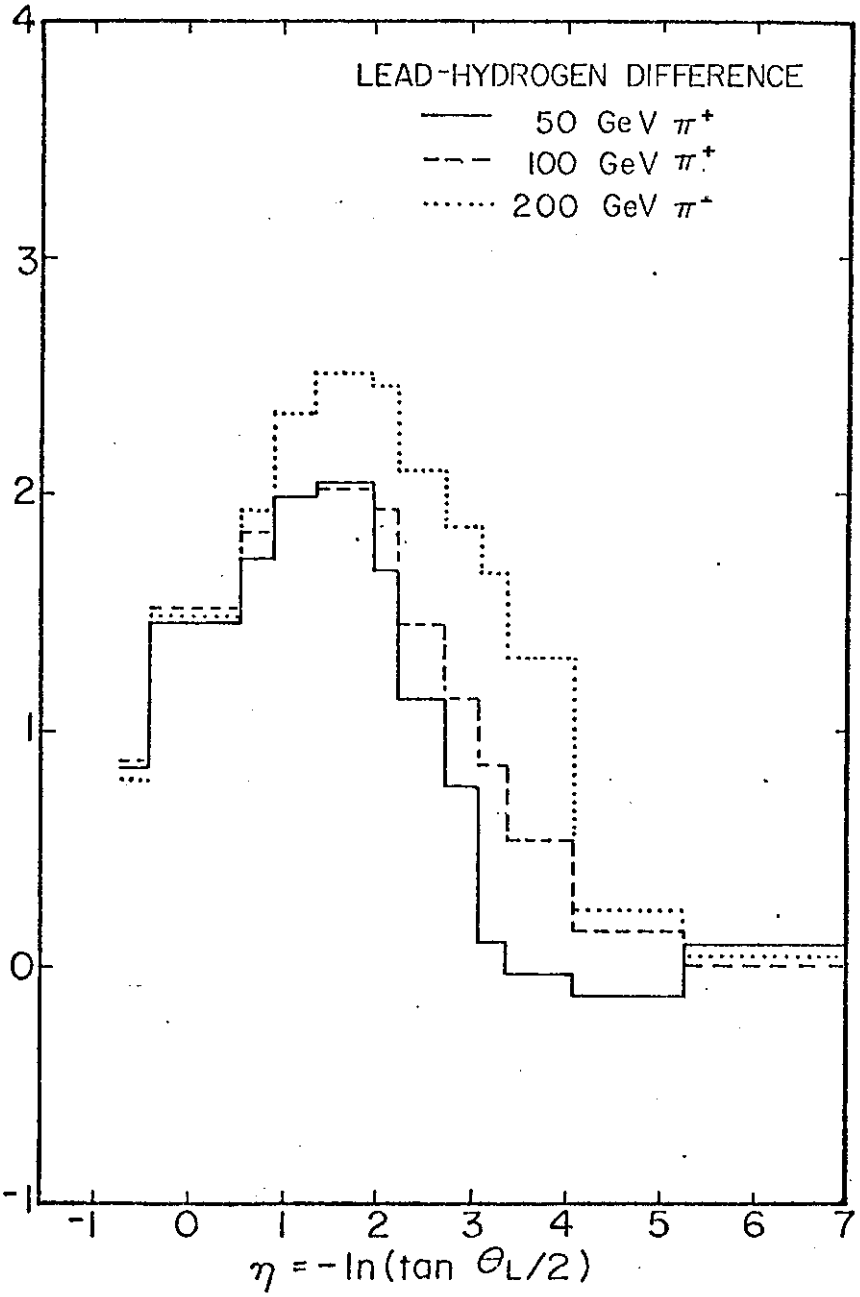
LEAD-HYDROGEN DIFFERENCE
50 GeV π+
100 GeV π+
200 GeV π+
4
3
2
1
0
-1
-1 0 1 2 3 4 5 6 7
η = - ln (tan θL/2)

Fig. 9

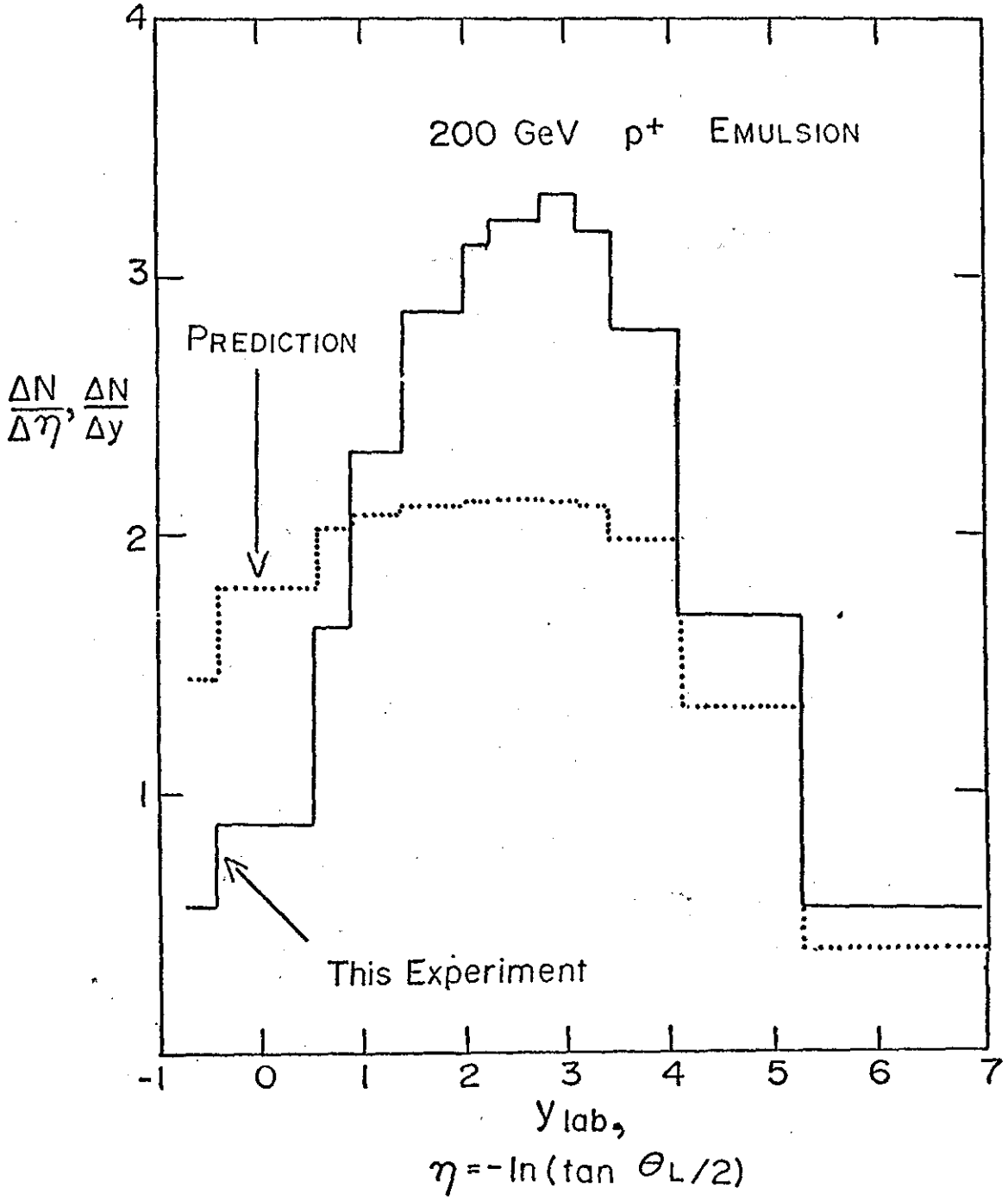
200 GeV p+ EMULSION
PREDICTION
This Experiment
ΔN/Δη, ΔN/Δy
y lab,
η = - ln (tan θL/2)
4
3
2
1
-1
0
1
2
3
4
5
6
7

Fig. 10